



# Photonicallly Generated Frequency Hopped Linear Frequency Modulated Signal Using a DFB Laser

Bikash Nakarmi , Senior Member, IEEE, Yansong Bai, Chuanqi Fang, Xiangchun Wang , Ukash Nakarmi , Ikechi Augustine Ukaegbu , Senior Member, IEEE, and Shilong Pan , Senior Member, IEEE

**Abstract**—Threats and security are critical issues in a multi-RADAR environment, which severely affect the performance metrics of a RADAR system, such as range resolution, false detection, and image quality. In a multi-RADAR environment, the issues of jamming, spoofing, and interferences should be considered for practical implementation. In this paper, we experimentally demonstrate a photonicallly generated frequency hopped linear frequency modulated (Ph-FHLMF) signal using injection locking in a DFB laser. For a proof of concept, we develop Ph-FHLMF with an eight-step and four-step hopping, each step having a bandwidth of 2 GHz and 1 GHz, respectively, and a total bandwidth of 8 GHz. The generated Ph-FHLMF signal detects two objects separated by 10, 5, and 2.5 cm with a maximum error of 3 mm. Further, for the proof of concept of the interference agility of the Ph-FHLMF signal, target objects are detected in the presence of an interferer, which is a conventional linear frequency modulated radar with the same/different bandwidths and chirps. Unlike in conventional LFM, the Ph-FHLMF signal overcomes the false detection and maintains a similar resolution in both scenarios, with and without an interferer.

**Index Terms**—Frequency hopping, interference, multi-radar environment, optical injection, semiconductor lasers.

## I. INTRODUCTION

**P**HOTONICS radio detection and ranging (Ph-RADAR) is one of the most studied fields in microwave photonics, which is mainly committed to improving the resolution of target detection and recognition; high-resolution imaging; monitoring, and electronic warfare (EW) operations [1]–[3]. Great efforts

have been made to improve radar functions using different techniques for radar applications in various fields, such as imaging, weather monitoring, defense, and autonomous vehicle [4], [5]. Photonics RADAR has become a suitable solution due to its inherent advantages, such as wide bandwidth, low loss, wavelength division multiplexing, immunity to electromagnetic interference, and an all-weather system [6], [7]. However, with an increasing number of applications of photonics RADAR, interference, spoofing, and jamming have become critical issues to be considered as they affect the overall performance of the RADAR, especially detection capability, range resolution, and response time of detection and imaging [8]–[11].

Among different kinds of Ph-RADAR based on the transmitting waveform, linear frequency modulation (LFM) based RADAR is widely used. LFM signal provides good pulse compression capability, inherent anti-electronic attack capability, and a relatively simple structure that offers high distance resolution and a wide detection range [12]–[15]. However, due to the simple waveform, LFM signals are prone to attacks from other modern electronic technology-based RADARs [16]–[18]. For example, an attacker can use similar hardware to the victim's radar to monitor the original radar signal and generate a similar signal, which acts as a spoofing [8]. Besides spoofing, interferences from other RADARs (mutual or non-mutual) and attacks from the intruders reduce the signal-to-noise ratio (SNR), resulting in a poor range resolution and poor detection capabilities and hence the imaging resolution of the LFM RADAR decreases [19]. As a result, radars that use LFM as transmission signals cannot cope with interference and deception in a multi-radar environment [20], [21]. Therefore, a new transmission signal is needed to solve this problem.

One of the possible new transmission signals is a frequency hopped LFM signal, which inherits the high-resolution detection and divides the total time interval into several sub-intervals of LFM signals. Owing to the nature of the frequency hopping sequences and the hopping steps that can be changed, the signals are not easily captured by intentional intrusion or unintentional interference by the intruders/interferers, which significantly improves the reliability of radar detection. Few researchers have theoretically proposed a technique to overcome the interference in the electronics domain but have not demonstrated a complete system to mitigate the interferences and intrusions [22]–[24]. Therefore, in this paper, we propose a photonicallly generated frequency hopped LFM (Ph-FHLMF) signal followed by detecting target objects in the presence of interferers. The basic

Manuscript received 27 February 2022; revised 22 April 2022 and 29 April 2022; accepted 6 May 2022. Date of publication 12 May 2022; date of current version 21 October 2022. This work was supported in part by the Nanjing University of Aeronautics and Astronautics under Grant 90YAH21066 and in part by Nazarbayev University Collaborative Research under Grant 11022021CRP1507. (Corresponding authors: Bikash Nakarmi; Shilong Pan.)

Bikash Nakarmi, Yansong Bai, Chuanqi Fang, Xiangchun Wang, and Shilong Pan are with the Key Laboratory of Radar Imaging and Microwave Photonics and Ministry of Education, Nanjing University of Aeronautics and Astronautics, Nanjing 210016, China (e-mail: bikash@nuaa.edu.cn; bys970911@nuaa.edu.cn; fangchuanqi@nuaa.edu.cn; wangxch@nuaa.edu.cn; pans@ieee.org).

Ukash Nakarmi is with the Department of Computer Science and Computer Engineering, University of Arkansas, Fayetteville, AR 72701 USA (e-mail: unakarmi@uark.edu).

Ikechi Augustine Ukaegbu is with the Integrated Device Solutions and Nanophotonics (iDSN) Laboratory, School of Engineering and Digital Sciences, Nazarbayev University, Nur-Sultan 010000, Kazakhstan (e-mail: ikechi.ukaegbu@nu.edu.kz).

Color versions of one or more figures in this article are available at <https://doi.org/10.1109/JLT.2022.3174664>.

Digital Object Identifier 10.1109/JLT.2022.3174664

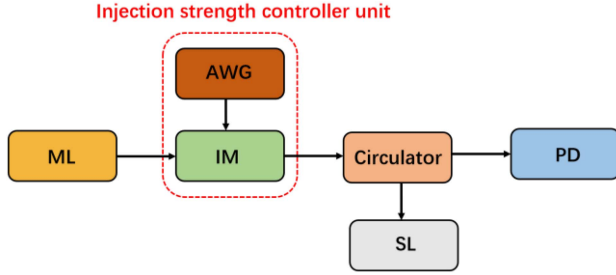


Fig. 1. Block diagram illustrating the photonic generated frequency hopped LFM signal. ML: master laser; AWG: arbitrary wave generator; IM: intensity modulator; SL: slave laser; PD: photodiode.

principle of the Ph-FHLFM signal generation is to inject a single light beam with changing intensity obtained through an arbitrary wave generator (AWG) into a distributed feedback (DFB) laser operating in a period one (P1) oscillation state [25], [26]. In this proposed scheme, rather than generating a complete chirp signal from the start frequency of the LFM signal to the stop frequency, it generates LFM signals with different start-stop frequencies in its subintervals. However, while doing it, attention should be taken to confirm that no overlapping and frequency gaps between generated LFM signals occur within a total period. This paper develops a Ph-FHLFM signal with four-step and eight-step frequency hopping within a total bandwidth of 8 GHz for a proof-of-concept demonstration. Further, a frequency hopped LFM signal with a four-step frequency hopping with a 2GHz bandwidth of each subinterval, totaling 8 GHz bandwidth (LFM1:8-10GHz, LFM2:14-16GHz, LFM3:12-14GHz, and LFM4:10-12GHz), is used to detect two target objects separated with a distance of 10 cm, 5 cm, and 2.5 cm in the absence and presence of interferences. In the experiment, we use the widely used LFM signal with the same/different BW and chirp to that of Ph-FHLFM as an interference signal. The results verify that the proposed Ph-FHLFM signal overcomes false detection and poor SNR and provides a similar range resolution even in the presence of interferers and intruders. Hence, the proposed scheme has a wide application for radars operating in a multi-RADAR environment such as defense, automobiles, and industries to mitigate security and safety threats.

## II. OPERATING PRINCIPLE

The basic operating principle of the proposed photonic generated frequency hopped LFM signal is the abrupt redshift of the emission mode of the DFB laser with an abrupt change in the power of the injected beam. Fig. 1 shows the basic block diagram illustrating the operating principle of the proposed Ph-FHLFM. In Fig. 1, the power of the master laser (ML) is modulated by the injection strength controller unit, which is comprised of the AWG and the intensity modulator, before injecting it into the slave laser (SL), which is the DFB laser. Based on the waveform of the AWG, the power of the ML is varied, and accordingly, the emission mode of the DFB laser is redshifted. Upon optical beating of the redshifted mode of the DFB laser and the injected beam through the photodiode (PD), which are the output of the DFB laser after the injection of ML into SL, the RF signal with

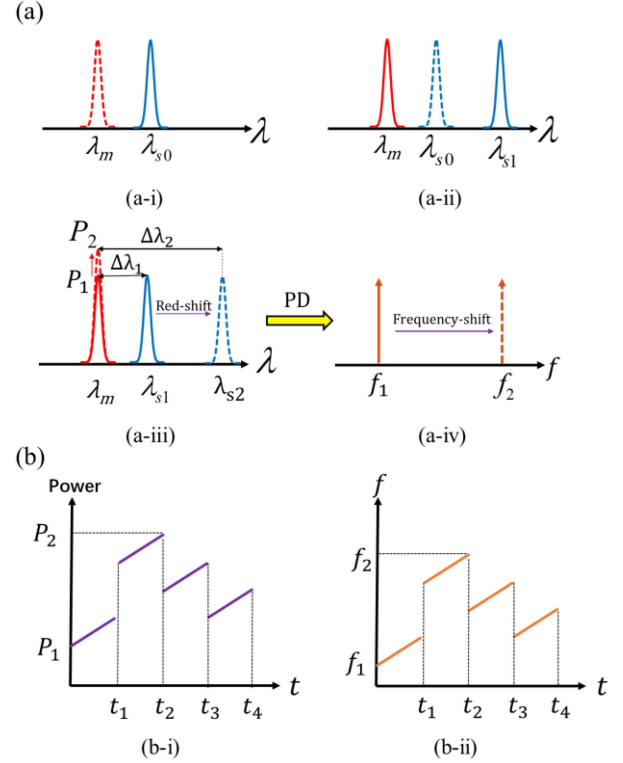


Fig. 2. Illustration of (a) Redshift in a DFB laser, (b) Generation of FHLFM signal.

varying frequencies can be observed. The wavelength detuning determines the starting frequency of the frequency varying RF signal, whereas the maximum amplitude of the AWG signal that modulates the power of the ML determines the maximum frequency shift.

Fig. 2 illustrates the basic operating principle using the schematic spectrum diagram. In Fig. 2(a)-(i), the blue line indicates the output emission wavelength of a DFB laser,  $\lambda_{s0}$ , without any injected beam, whereas the red line indicates the wavelength of the injected beam, ML,  $\lambda_m$ . Injecting ML with the proper power and wavelength detuning, the redshift phenomena on the emission mode of the DFB laser from  $\lambda_{s0}$  to  $\lambda_{s1}$  is observed as shown in Fig. 2(a)-(ii). On continuous change in the injected beam power from  $P_1$  to  $P_2$ , the emission mode of the DFB laser shifts from  $\lambda_{s1}$  to  $\lambda_{s2}$  accordingly, as shown in Fig. 2(a)-(iii), where the arrow indicates the shifting of power and wavelength. On optical beating between the ML and the redshifted emission mode of SL in a PD, RF signal with varying frequency, from  $f_1$  to  $f_2$ , can be observed as shown in Fig. 2(a)-(iv). Instead of changing the amplitude of the AWG signal linearly, the amplitude of AWG can be changed abruptly within a specific time interval. Fig. 2(b)-(i) illustrates several abrupt changes in the power within a time interval rather than changing linearly throughout the time interval. Implementing the abrupt amplitude change of the AWG signal, the modulation in the power of the ML is obtained, and as a result, the output frequency changes abruptly on optical beating, as shown in Fig. 2(b)-(ii). The number of hopping and the sequence of FHLFM signals are dependent on the number and sequences

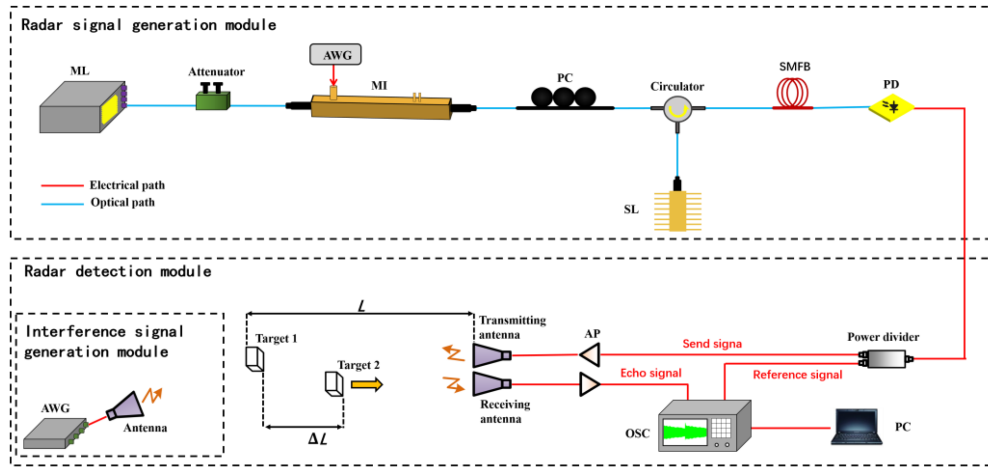


Fig. 3. Experiment setup for detecting the objects using proposed Ph-FHLMF signal with and without interferers.

of abrupt changes in input power, whereas the time interval for linear variation of the RF signal is dependent on the time interval of linear change in the power. In Fig. 2(b)-(i), an abrupt change occurs after equal sub-time intervals, and as a result, a linear frequency modulating signal can be generated between sub-time intervals generating the FHLFM signal as illustrated in Fig. 2(b)-(ii).

### III. EXPERIMENTAL SETUP AND RESULTS

The experimental setup for the proposed Ph-FHLMF signal generation and its implementation for detecting objects in the absence and presence of interference is shown in Fig. 3. The basic operating principle of the proposed scheme is the redshift in the SL upon injecting a beam with varying optical power. The slave laser used in the experiment is a DFB laser (Actech LD15DM) and is biased with a biasing current of 30 mA and an operating temperature of 25 °C. The DFB laser has an emission wavelength of 1542.04 nm with these biasing conditions. The tunable laser, Agilent N7714A, which can tune the wavelength from 1520 nm to 1600 nm and the power from 5.5 dBm to 16.0 dBm, is used as the ML to inject the beam into the DFB laser. The wavelength of ML is varied depending on the requirement in analyzing redshift in the emission of a DFB laser with different wavelength detuning. For the generation of LFM, Ph-FHLMF, and target object detecting experiments, the ML is set at the wavelength of 1541.99 nm. As a result, the Ph-FHLMF with a starting frequency of 8.0 GHz is obtained on the optical beating of the injected beam and the emission mode of the slave laser in a photoelectrical detector (PD). The PD (u2t XPDV2120RA) with a 3-dB bandwidth of 40 GHz is used in the experiment. The polarization controller in the experiment is used to maintain the TE polarization required for injection locking phenomena. The attenuator is used to reduce the power of the ML for analyzing its effect on redshift. The intensity controller, which is the central unit, is used to control the power of the injected beam and consists of an arbitrary wave generator (AWG, 120 MHz, Agilent 85110A) and a Mach-Zehnder modulator (Lucent 2623NA) with a maximum modulation rate of 10 Gb/s. Based upon the AWG

waveform, the power of ML is modulated by the MZM and is injected into the SL. Hence, a redshift in the emission frequency of SL is observed. With an abrupt change of the AWG waveform, an abrupt redshift is observed. Hence, upon optical beating between abrupt redshifted emission frequency and the injected beam, the Ph-FHLMF is generated.

For a proof of concept demonstration of the interference handling capability of the generated Ph-FHLMF signal, an LFM signal with the same/different BWs and chirps to that of FHLFM is used as an interferer in the experiment. Two target objects with separation distances,  $\Delta L$ , of 10, 5, and 2.5 cm, are detected with and without interference at the  $L = 3.55$  m, as shown in Fig. 3. This experiment consists mainly of three parts: (a) analysis of the frequency shifting of emission mode of the SL upon a change in optical power of the injected beam for different wavelength detuning, (b) generation of Ph-FHLMF signal, and (c) detection of target objects in the absence and presence of the interference using the proposed Ph-FHLMF.

#### A. Analysis of Redshift in the Emission Mode of a DFB Laser

In this section, we analyze the redshift of the emission wavelength of the DFB laser with a change in the input injected power for different wavelength detuning. The redshift in the emission wavelength of the slave laser with a change in the intensity of the injected beam is the primary technique for obtaining the LFM signal at the output. In the analysis, we set the emission mode of the DFB laser as constant at the wavelength of 1542.04 nm, and the wavelength of ML is varied to obtain different wavelength detunings. The wavelength detuning determines the starting frequency of the output RF signal. At the same time, the total redshift of the emission mode determines the bandwidth obtained through the change in the injected optical power. We inject the ML into the SL without the AWG and the modulator to observe the shift in the emission wavelength of the SL. The power of the input injected beam is varied by using an optical attenuator. Fig. 4 shows the effect of varying the intensity of the injected beam. At first, we set the wavelength detuning,  $\Delta\lambda$ , to 0.09 nm and then varied the power of the injected beam from



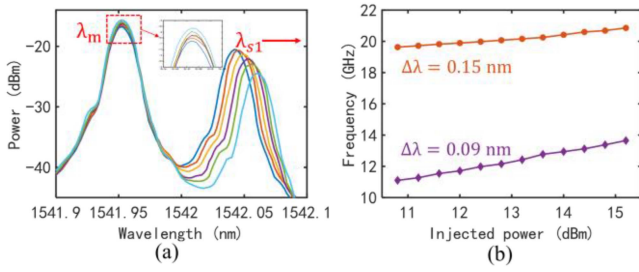


Fig. 4. Effect of the change in the optical power of the injected beam at the output of the DFB laser (a) Optical spectrum at the output of DFB (b) Frequency variation for different wavelength detuning.

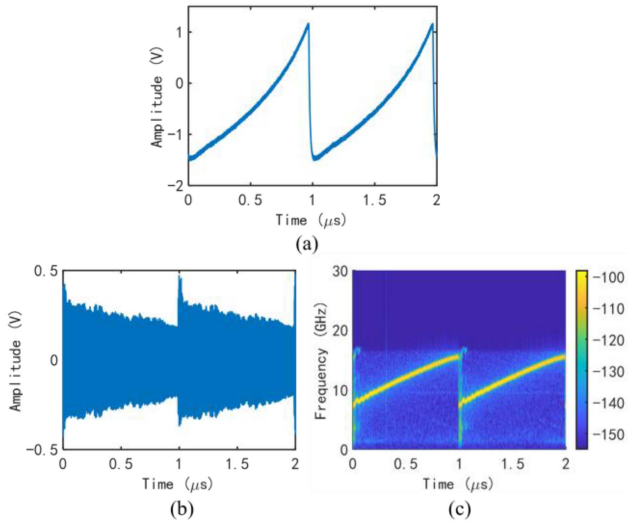


Fig. 5. Input and output of the waveform LFM generator (a) AWG signal used to modulate the injected beam, ML (b) Temporal waveform of the generated LFM signal, and (c) Frequency versus time waveform of the generated LFM signal.

-16.75 dBm to -15.50 dBm in the step of 0.25 dBm. The redshift in emission wavelength of the DFB laser with a change in optical power is illustrated in Fig. 4(a). On optical beating in PD, the change in RF frequency is observed, as shown in Fig. 4(b). In Fig. 4(b), the change in the output frequency for  $\Delta\lambda = 0.15$  nm is also presented. We can see from Fig. 4(b) that with a change in the wavelength detuning, the starting frequency is changed. It should be noted that the shift in the output RF frequency, which is due to the redshift in the emission frequency of the DFB laser, is slightly nonlinear with the linear change in the power of the injected beam. The nonlinear change is due to the nonlinear dynamics of the SL upon injection of an external beam. Hence, instead of a sawtooth signal, a sawtooth-like AWG signal, as illustrated in Fig. 5(a), is required to obtain a linearly varying RF signal at the output. Fig. 5(b) and (c) show the temporal waveform and the instantaneous frequency-time diagram of the generated LFM signal, respectively when the AWG signal shown in Fig. 5(a) is applied to the modulator. The total bandwidth of 8 GHz (from 8 GHz to 16 GHz) LFM signal is observed in the oscilloscope after signal processing.

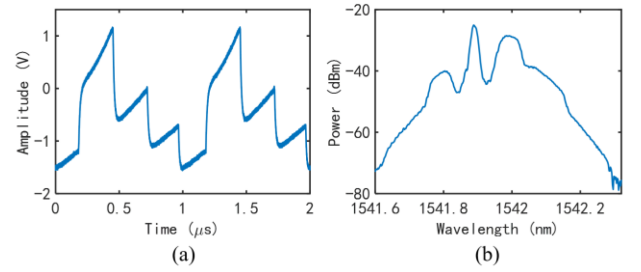


Fig. 6. (a) The AWG signal for random hopped LFM signal (b) Optical spectrum.

### B. Generation of Frequency Hopped LFM Signal

The redshift analysis of the emission mode of SL in Section III(A) is used for determining the relation between the amplitude of the electric AWG signal and the frequency shifting of the RF signal at the output. Using the relationship between the amplitude of AWG and the frequency of the RF signal, the output frequency can be hopped by an abrupt change in the amplitude of AWG. This section demonstrates the generation of a Ph-FHLFM signal using the injection of an external beam into the DFB laser, as shown in Fig. 3. The external beam has an abrupt intensity change which is made possible by the variation of the AWG signal. In this experimental setup for generating Ph-FHLFM, the biasing conditions of the DFB laser are kept the same, and the ML is set at the wavelength of 1541.99 nm. The AWG waveform is changed in this section to obtain the FHLFM signal. At first, the total time interval of the AWG signal is divided into four subintervals so that a four-step hopping can be obtained at the output. Then, instead of generating a continuously increasing amplitude of the AWG signal, the amplitude of the AWG waveform is abruptly changed between the subintervals. Since the AWG amplitude is abruptly changed between the subintervals, the output frequency of the RF signal also varies abruptly. The change in RF frequency with the change in amplitude of the AWG signal is discussed in the previous section. To confirm no overlap and gaps in the generated RF signal, we ensure no overlap and gaps in the start and stop amplitudes of AWG between the subintervals.

In the experiment, we set the total and subinterval bandwidth of the RF output as 8 GHz (8 to 16 GHz) and 2GHz for four-step hopping Ph-FHLFM, respectively. The total bandwidth of Ph-FHLFM is determined by the total redshift of emission frequency of the DFB laser, which is due to the amplitude varying AWG signal within the interval. In Fig. 6(a), the abrupt change in the amplitude of the AWG signal is observed at the subintervals of  $0.25\mu\text{s}$ . Also, there is no amplitude overlap and gaps between the subintervals (-1.5 to -1.18, 0 to 1.2, -0.71 to 0, and -1.18 to -0.71 V). The corresponding optical spectrum at the output of DFB is shown in Fig. 6(b). On optical beating of the output of the DFB laser in a PD, the Ph-FHLFM signal can be observed, as shown in Fig. 7. Fig. 7(a) shows the instantaneous temporal waveform of Ph-FHLFM, where the total period and subinterval periods are matched with that of the AWG signal. Fig. 7(b) shows the frequency-time diagram of the generated PH-FHLFM signal, which consists of four LFM signals (LFM1:8.0–10.0 GHz,

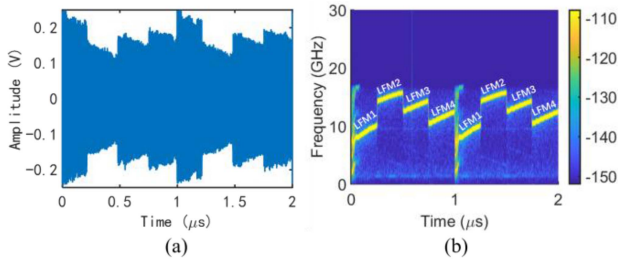


Fig. 7. Generated four-step FHLFM signal (a) the instantaneous waveform (b) the corresponding frequency-time diagram.

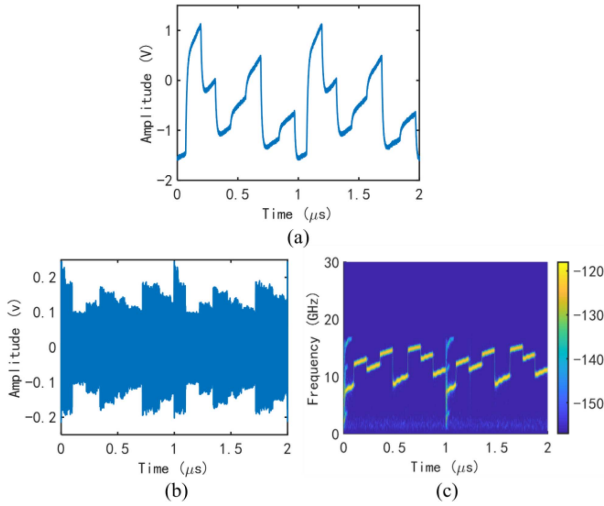


Fig. 8. Generated eight-step FHLFM signal (a) Applied AWG signal (b) the instantaneous waveform (c) Corresponding frequency-time diagram.

LFM2:14.0–16.0 GHz, LFM3:12.0–14.0 GHz, and LFM4:10.0–12.0 GHz) which are hopped corresponding to the AWG signal applied. Each LFM in the subinterval has a bandwidth of 2 GHz, totaling a bandwidth of 8 GHz. The hopping sequence of the Ph-FHLFM can be modified by controlling the abrupt change in AWG signal between the respective subinterval.

Further, to demonstrate the reconfigurability of the number of hopping steps in the Ph-FHLFM signal using the proposed method, the AWG signal is modified with eight abrupt amplitude changes within the total time interval of  $1\mu\text{s}$ , as illustrated in Fig. 8(a). Hence, eight-step frequency hopping is obtained. The instantaneous waveform and frequency-time diagram of the corresponding Ph-FHLFM are illustrated in Fig. 8(b) and (c), respectively. As we can see from Fig. 8, the generated signal has the same total bandwidth of 8 GHz (from 8.0 – 16.0 GHz) because the minimum and maximum amplitude of the AWG signal within a full-time interval,  $T$  of  $1\mu\text{s}$ , is the same, from -1.5 V to 1.2 V, to that of four-step frequency hopping. Also, all the LFM signals in subintervals have an equal bandwidth of 1GHz. The only difference is the number of hopping and the order of frequency hopping of the Ph-FHLFM signal. The number of hopping depends on the total number of subintervals, and the hopping sequence depends on the sequence of the abrupt change in the amplitude of the AWG signal between the subintervals.

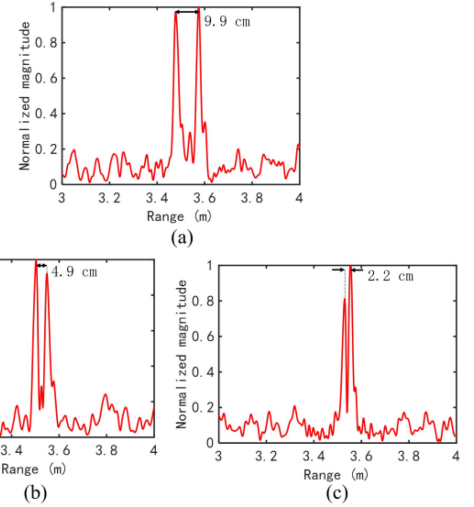


Fig. 9. The measured results with Ph-FHLFM without interference: actual separation distance of two target distance difference (a) 10 cm (b) 5 cm (c) 2.5 cm.

### C. Detection of Target Objects With and Without Interference Using Proposed Ph-FHLFM

As a proof-of-concept demonstration of the interference-agile capability of the Ph-FHLFM, the generated Ph-FHLFM signal is used to detect two objects separated by different distances in the absence and presence of interference. At first, two objects separated with  $\Delta L$  of 10, 5, and 2.5 cm are detected using the proposed Ph-FHLFM without interference and then with interference. For the experiment, Target 1 is placed at the distance,  $L$ , 3.55 m, from the RADAR antenna, as shown in Fig. 3. For the measurement and detection of target objects with different separation distances, Target 2 is moved, putting Target 1 stationary. We used the Ph-FHLFM signal with four-step hopping for the detection of target objects. In order to measure the distance between the two objects, the generated Ph-FHLFM is divided into two paths using an electrical power divider. One path is sent to the LNA (low noise amplifier) and then transmitted by a transmitting antenna, and the other path is used as the reference signal. The echo signal received by the receiving antenna is amplified by the LNA and observed in the oscilloscope. Finally, the separation distance of the two objects is calculated using a digital processing algorithm that calculates the delay of the received signal and then changes the result to the distance information. Fig. 9 shows the cross-correlation of the transmitted and the received echo signal. The peaks in the cross-correlation represent the number of objects within the range of interest, whereas the separation of two peaks shows the separation distance,  $\Delta L$ . Fig. 9(a), (b), and (c) show the cross-correlation functions when the target objects are separated by 10, 5, and 2.5 cm, with an error of 0.1, 0.1, and 0.3 cm, respectively.

Next, we detected the target objects in the presence of interference. A conventional LFM signal with the same/different bandwidth and chirp is used as an interferer, as shown in Fig. 10. At first, the interference signal with the same bandwidth and

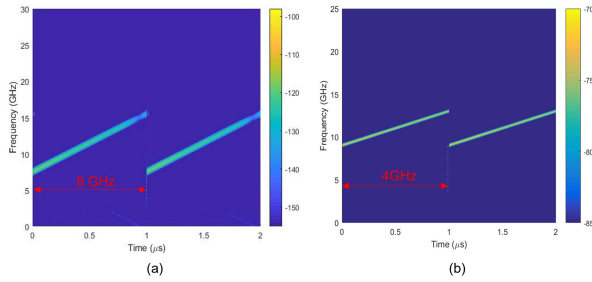


Fig. 10. The interference signal of (a) Same total BW and chirp rate, 8 GHz, 8 GHz/ $\mu$ s (b) Different total BW and chirp, 4 GHz, 4 GHz/ $\mu$ s.

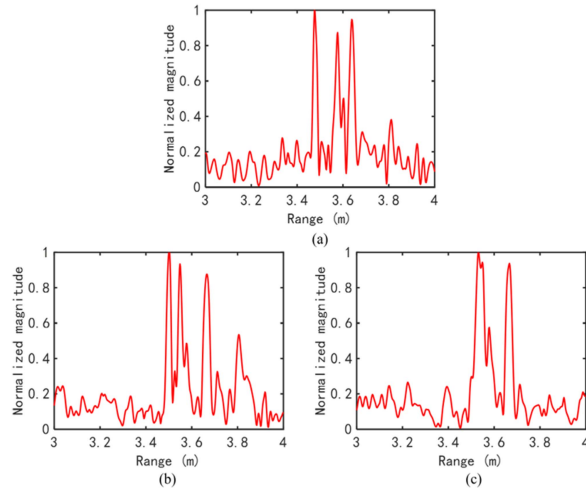


Fig. 11. The measured results with LFM radar in the presence of interference signal, same BW and chirp, 8 GHz and 8 GHz/ $\mu$ s: actual separation distance of two targets are (a) 10 cm (b) 5 cm (c) 2.5 cm.

chirp of 8 GHz and 8 GHz/ $\mu$ s, respectively, as that of Ph-FHLFM is used for the interference signal as shown in Fig. 10(a). Fig. 10(b) shows the interference signal with different bandwidth and chirp of 4 GHz and 4 GHz/ $\mu$ s, respectively, from that of Ph-FHLFM. The interference signal with the same bandwidth and chirp, which acts as the worst interference scenario and provides false detection [8], is used first; and then followed by the interference with different bandwidth and different chirp. In both interference scenarios, the interferer is placed in the direction of the receiving antenna. Before detecting the target objects with a Ph-FHLFM signal, we use LFM-based radar to detect the objects in the presence of an interferer.

Fig. 11 shows the cross-correlation of the transmitted conventional LFM radar signal and received signals with two target objects separated by 10 cm, 5 cm, and 2.5 cm when the interference signal is of the same bandwidth and chirp as that of the transmitted signal. Due to the interferer, the cross-correlation, which gives the range of objects, shows multiple peaks (more than two), unlike in Fig. 9. The multiple peaks in Fig. 11 show that multiple objects are present in the area of interest, which is false. We observed that even though only two target objects are present in the detection area, the number of peaks observed is different for different separation distances between the objects. This change in the number of peaks is due

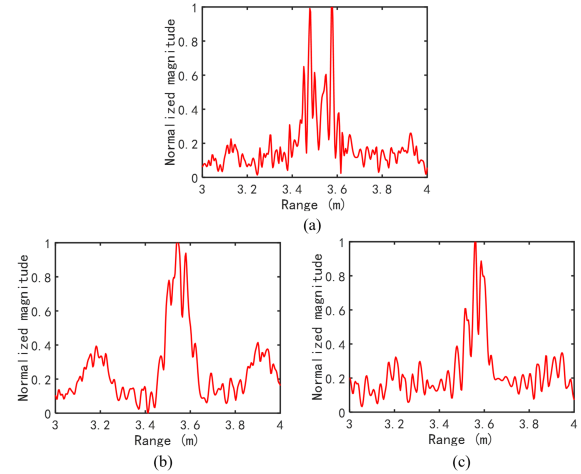


Fig. 12. The measured results with LFM radar in the presence of interference signal with different BW and chirp, 4 GHz and 4 GHz/ $\mu$ s: actual separation distance of two targets are (a) 10 cm (b) 5 cm (c) 2.5 cm.

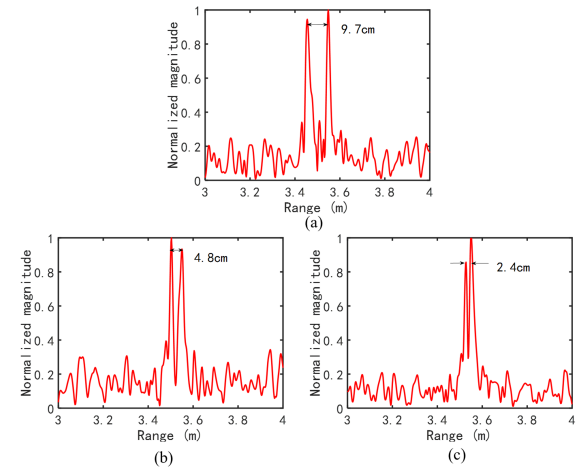


Fig. 13. The measured results with Ph-FHLFM in the presence of interference signal, same total BW and chirp, 8 GHz and 8 GHz/ $\mu$ s: actual separation distance of two targets are (a) 10 cm (b) 5 cm (c) 2.5 cm.

to a change in received interference signals because of different separation distances between the targets. Next, an interference signal, as illustrated in Fig. 10(b), with different bandwidth and chirp, is used. We observed that the noise floor increases even though few peaks are observed, as shown in Fig. 12, compared to those with the same bandwidth and the chirp. Fig. 11 and 12 shows that LFM RADAR cannot mitigate interference while detecting the target objects in an interference environment. To overcome it, we use our proposed scheme of Ph-FHLFM instead of the conventional LFM RADAR.

Finally, we demonstrate the detection capability of our proposed Ph-FHLFM in the presence of interference as a proof of concept. For this purpose, we used the same interferers, as shown in Fig. 10, that are used to detect target objects by LFM RADAR. Figs. 13 and 14 show the cross-correlation function in the presence of the interference with the same total BW and chirp (8 GHz, 8 GHz/ $\mu$ s) and different total BW and chirp (4 GHz, 4 GHz/ $\mu$ s), respectively, using our proposed Ph-FHLFM.



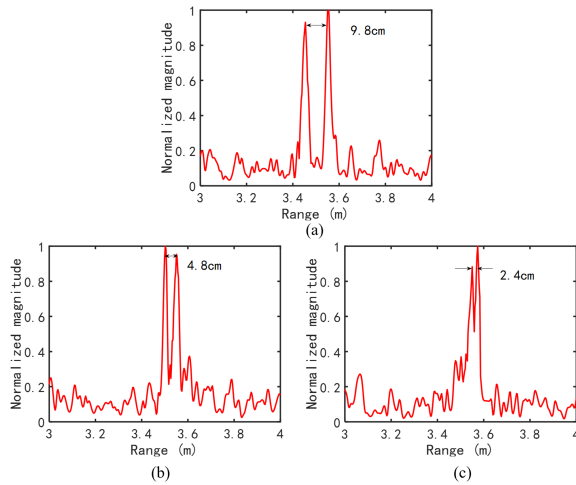


Fig. 14. The measured results with PH-FHLMF in the presence of interference signal, different total BW and chirp, 4 GHz and 4 GHz/ $\mu$ s, environment: actual separation distance of two targets are (a) 10 cm (b) 5 cm (c) 2.5 cm.

There are no significant changes in cross-correlation for object detection with both types of interference signals and are similar to that of Fig. 9, without any interference. The cross-correlation functions presented in Figs. 13 and 14 verify that the proposed scheme can mitigate the interferer, unlike in the conventional LFM, where false detection and an increase in noise floor are observed. Using our proposed Ph-FHLMF, the difference between the actual value and measured value for two target objects with the separation distances of 10 cm, 5 cm, and 2.5 cm in the presence of the interference signals, Fig. 10(a) and (b), are 0.3 cm, 0.2 cm, and 0.1 cm for Fig. 10(a); and 0.2 cm, 0.2 cm, and 0.1 cm for Fig. 10(b), respectively. More importantly, the detection of objects with Ph-FHLMF is not affected by the interference signal, which demonstrates the anti-interference capability of the proposed Ph-FHLMF.

#### IV. CONCLUSION

In this paper, we experimentally demonstrated a photonic generated frequency hopped linear frequency modulated signal using the injection of an external beam in a DFB laser. The total time interval is divided into several equal subintervals. An abrupt amplitude-changed AWG signal is used in each subinterval rather than applying the almost linear waveform from AWG for a whole time interval period to generate the Ph-FHLMF signal. Using the techniques of abrupt redshift through the modification of the AWG waveform, the Ph-FHLMF signal with the total bandwidth of 8 GHz and the hopping step of eight and four are demonstrated. The number of hopping steps of the Ph-FHLMF depends on the number of abrupt changes in the amplitude of the AWG signal, whereas the total bandwidth depends on the total redshift of the emission frequency of the DFB laser. The generated Ph-FHLMF signal has a start frequency of 8 GHz and a stop frequency of 16 GHz. The starting frequency can be changed by changing the wavelength detuning. The generated Ph-FHLMF signal with the four-step hopping (LFM1: 8.0 – 10.0 GHz, LFM2: 14.0 – 16.0 GHz, LFM3: 12.0 – 14.0 GHz, and

LFM4: 10.0 – 12.0 GHz) is used for detecting objects with various separation distances in the absence and presence of the interferers. We also verify that dividing the total bandwidth into sub-interval bandwidth with an abrupt change between the subintervals does not affect the detection range resolution of the RADAR. The range resolution is not changed because the total bandwidth of the Ph-FHLMF signal is the same within the total period, and no overlap and gaps of frequencies occur. An LFM radar with the bandwidth and chirp of 8 GHz and 8 GHz/ $\mu$ s and 4 GHz and 4 GHz/ $\mu$ s are used as an interferer. As a proof of concept demonstration, we verified that the proposed Ph-FHLMF mitigates both interference scenarios with a maximum range resolution error of 3 mm, unlike in the conventional LFM RADAR, where false detection and an increase in noise floor are observed. With the analysis done in this work on the detection capability of Ph-FHLMF, the proposed Ph-FHLMF can be used in various applications such as autonomous vehicles and defense RADARs applications to reduce safety and security threats.

#### REFERENCES

- [1] H. Zmuda and E. N. Toughlian, *Photonic Aspects of Modern Radar*, Norwood, MA, USA: Artech House, 1994.
- [2] J. Yao, "Microwave photonics," *J. Lightw. Technol.*, vol. 27, no. 3, pp. 314–335, Feb. 2009.
- [3] R. A. Minasian, "Photonic signal processing of microwave signals," *IEEE Trans. Microw. Theory Techn.*, vol. 54, no. 2, pp. 832–846, Feb. 2006.
- [4] G. Simonis, "Photonics in homeland and national security," *Conf. Lasers Electro-Opt./Int. Quantum Electron. Conf. Photon. Appl. Syst. Technol.*, America, USA: Optica Publishing Group, 2004, Art. no. PTuA2.
- [5] J. Dong, F. Zhang, Z. Jiao, Q. Sun, and W. Li, "Microwave photonic radar with a fiber-distributed antenna array for three-dimensional imaging," *Opt. Exp.*, vol. 28, pp. 19 113–19 125, 2020.
- [6] S. Pan and Y. Zhang, "Microwave photonic radars," *J. Lightw. Technol.*, vol. 38, pp. 5450–5484, 2020.
- [7] Y. Wang *et al.*, "Simultaneous detection of the distance and direction for a noncooperative target based on the microwave photonic radar," *Opt. Exp.*, vol. 29, pp. 31 561–31 573, 2021.
- [8] S. Alland, W. Stark, M. Ali, and M. Hegde, "Interference in automotive radar systems: Characteristics, mitigation techniques, and current and future research," *IEEE Signal Process. Mag.*, vol. 36, no. 5, pp. 45–59, Sep. 2019.
- [9] I.-P. Hwang, S.-J. Yun, and C.-H. Lee, "Mutual interferences in frequency-modulated continuous-wave (FMCW) lidars," *Optik*, vol. 220, 2020, Art. no. 165109.
- [10] L. Neng-Jing and Z. Yi-Ting, "A survey of radar ECM and ECCM," *IEEE Trans. Aerosp. Electron. Syst.*, vol. 31, no. 3, pp. 1110–1120, Jul. 1995.
- [11] A. L. Diehm, M. Hammer, M. Hebel, and M. Arens, "Mitigation of crosstalk effects in multi-LiDAR configurations," in *Proc. SPIE Electro-Opt. Remote Sens. XII*, 2018, Art. no. 1079604.
- [12] H. Chen, B. Nakarmi, and S. Pan, "Multi-band LFM signal with unidentical bandwidths subjected to optical injection in a DFB laser," *IEEE Photon. Technol. Lett.*, vol. 33, no. 8, pp. 391–394, Apr. 2021.
- [13] P. Zhou, F. Zhang, Q. Guo, and S. Pan, "Linearly chirped microwave waveform generation with large time-bandwidth product by optically injected semiconductor laser," *Opt. Exp.*, vol. 24, pp. 18 460–18 467, 2016.
- [14] H. Chen, P. Zhou, L. Zhang, S. Bassi, B. Nakarmi, and S. Pan, "Reconfigurable identical and complementary chirp dual-LFM signal generation subjected to dual-beam injection in a DFB laser," *J. Lightw. Technol.*, vol. 38, no. 19, pp. 5500–5508, Oct. 2020.
- [15] Q. Guo, F. Zhang, P. Zhou, and S. Pan, "Dual-band LFM signal generation by optical frequency quadrupling and polarization multiplexing," *IEEE Photon. Technol. Lett.*, vol. 29, no. 16, pp. 1320–1323, Aug. 2017.
- [16] F. Uysal and S. Sanka, "Mitigation of automotive radar interference," in *Proc. IEEE Radar Conf.*, 2018, pp. 0405–04 103.
- [17] J. Bechter, M. Rameez, and C. Waldschmidt, "Analytical and experimental investigations on mitigation of interference in a DBF MIMO radar," *IEEE Trans. Microw. Theory Techn.*, vol. 65, no. 5, pp. 1727–1734, May 2017.

- [18] F. Uysal, "Phase-coded FMCW automotive radar: System design and interference mitigation," *IEEE Trans. Veh. Technol.*, vol. 69, no. 1, pp. 270–281, Jan. 2020.
- [19] E. Yeh *et al.*, "Security in automotive radar and vehicular networks," *Microw. J.*, vol. 60, no. 5, pp. 148–164, 2017.
- [20] J. Liu, Y. Zhang, and X. Dong, "Linear-FM random radar waveform compressed by dechirping method," *IET Radar Sonar Navigation*, vol. 13, pp. 1107–1115, 2019.
- [21] D. L. Adamy, *EW 104: Electronic Warfare Against a New Generation of Threats.*, Norwood, MA, USA: Artech House, 2015.
- [22] A. Roy, H. B. Nemade, and R. Bhattacharjee, "Radar waveform diversity using nonlinear chirp with improved sidelobe level performance," *AEU-Int. J. Electron. Commun.*, vol. 136, 2021, Art. no. 153768.
- [23] T. Moon, J. Park, and S. Kim, "BlueFMCW: Random frequency hopping radar for mitigation of interference and spoofing," *EURASIP J. Adv. Signal Process.*, vol. 2022, no. 1, pp. 1–17, 2022.
- [24] S. D. Blunt *et al.*, "Principles and applications of random FM radar waveform design," *IEEE Aerosp. Electron. Syst. Mag.*, vol. 35, no. 10, pp. 20–28, Oct. 2020.
- [25] S.-C. Chan, S.-K. Hwang, and J.-M. Liu, "Period-one oscillation for photonic microwave transmission using an optically injected semiconductor laser," *Opt. Exp.*, vol. 15, pp. 14 921–14 935, 2007.
- [26] B. Nakarmi *et al.*, "Linear frequency modulated photonics RADAR using injection locking in semiconductor laser," in *Proc. Int. Conf. Electron., Commun. Inf. Technol.*, 2021, pp. 1–4.

**Bikash Nakarmi** (Senior Member, IEEE) received the B.E. degree in electronics and communication from Tribhuvan University, Kirtipur, Nepal, in 2008, the M.E. degree in information and communication engineering from Harbin Engineering University, Harbin, China, in 2004, and the Ph.D. degree from the Korea Advanced Institute of Science and Technology (KAIST), Daejeon, South Korea, in 2012. In 2016, he joined the College of Electronics and Information Engineering, Nanjing University of Aeronautics and Astronautics, China, where he is currently a Professor with the Key Laboratory of Radar Imaging and Microwave Photonics, Ministry of Education. From 2012 to 2013, he was a Research and Development Manager with InLC Technology Korea, a Postdoctoral Researcher with Nanjing University, Nanjing, China, during 2012–2014. From 2014 to 2016, he was a Research Professor with KAIST. He has authored and coauthored more than 75 research papers, including 40 peer-reviewed journals, 35 papers in conference proceedings and several invited talks. His research interests include developing optical blocks used in optical communication and networks using Fabry-Pérot laser diode, bio-sensors based on nano-structures, and microwave photonics.

He is a Senior Member of the Optical Society of America. Prof. Nakarmi was a committee Member in SPIE photonics ASIA 2012, IEEE ICECIT 2021, and a reviewer of several peer-reviewed journals.

**Yansong Bai** received the B.S. degree in electronic information engineering from the Jincheng College, Nanjing University of Aeronautics and Astronautics, Nanjing, China. He is currently working toward the master's degree in electronics engineering with the Nanjing University of Aeronautics and Astronautics.

His research focuses on the areas of semiconductor laser diodes applications for microwave photonics.

**Chuanqi Fang** received the B.S. degree in electronic information engineering from Anhui Normal University, Wuhu, China, in 2019. He is currently working toward the master's degree in electronics engineering with the Nanjing University of Aeronautics and Astronautics, Nanjing, China. His research focuses on the areas of semiconductor laser diodes applications for microwave photonics.

**Xiangchun Wang** received the B.Eng. degree in automation and the Ph.D. degree in microelectronics and solid-state electronics from Nanjing University, Nanjing, China, in 2009 and 2015, respectively. He is currently an Associate Professor with the Key Laboratory of Radar Imaging and Microwave Photonics, Ministry of Education, Nanjing University of Aeronautics and Astronautics, Nanjing, China. He has authored or coauthored more than 60 research papers, including more than 32 peer-reviewed journals and 28 papers in conference proceedings. His research interests include microwave photonics measurement and optical fiber sensing technologies.

**Ukash Nakarmi** received the B.E. degree in electronics and communication from Tribhuvan University, Kirtipur, Nepal, in 2008, the M.S. in electrical engineering from Oklahoma State University, Stillwater, OK, USA, in 2011, and the Ph.D. degree in electrical engineering from the State University of New York at Buffalo, Buffalo, NY, USA, in 2018. From 2018 to 2020, he was a Postdoctoral Fellow with the Department of Electrical Engineering and the Department of Radiology, Stanford University, Stanford, CA, USA, before joining the Department of Computer Science and Computer Engineering, University of Arkansas, Fayetteville, AR, USA, as an Assistant Professor.

His research interests include machine learning, big data, and signal processing with applications to computational imaging, radiology, and knowledge discovery from the data. His expertise lies in high dimensional data representation and reconstruction: encompassing techniques, such as compressed sensing, sparse representation, nonlinear representation, and manifold learning.

Dr. Nakarmi is a reviewer for several IEEE journals, including the IEEE TRANSACTIONS ON MEDICAL IMAGING and IEEE TRANSACTIONS ON COMPUTATIONAL IMAGING. He was a PC member in IEEE International Conference on Big Data 2021 and 2022.

**Ikechi Augustine Ukaegbu** (Senior Member, IEEE) received the B.Sc. degree in electrical engineering, electromechanics, and electro-technology and the M.Sc. degree in electronics and microelectronics from Moscow Power Engineering Institute, Technical University, Moscow, Russia, in 2004 and 2006, respectively, and the Ph.D. degree from the Korea Advanced Institute of Science and Technology (KAIST), Daejeon, South Korea, in 2012. From 2012 to 2013, he has been a Postdoctoral Researcher with Electrical Engineering Department, KAIST. From 2008 to 2009, he held R&D positions with Electronics and Telecommunications Research Institute, South Korea, and with Lightron Fiber-Optics Inc., South Korea, in 2013. From 2013 to 2016, he was also a Senior Engineer with Design Technology Team, Samsung Electronics Co. Ltd, South Korea. He co-founded a startup company, where he was the CTO from 2016 to 2017. Since 2018, he has been an Assistant Professor with the Electrical and Computer Engineering Department, School of Engineering, Nazarbayev University, Nur-Sultan, Kazakhstan. He is the Director of Integrated Device Solutions and Nanophotonics Laboratory, Nazarbayev University. His research interests include circuits and systems, microwave and nanophotonics, signal and power integrity, channel modeling, and sub-terahertz chip-to-chip links.

**Shilong Pan** (Senior Member, IEEE) received the B.S. and Ph.D. degrees in electronics engineering from Tsinghua University, Beijing, China, in 2004 and 2008, respectively. From 2008 to 2010, he was a "Vision 2010" Postdoctoral Research Fellow with the Microwave Photonics Research Laboratory, University of Ottawa, Ottawa, ON, Canada. In 2010, he joined the College of Electronic and Information Engineering, Nanjing University of Aeronautics and Astronautics, Nanjing, China, where he is currently a Full Professor and the Deputy Director of the Key Laboratory of Radar Imaging and Microwave Photonics, Ministry of Education.

He has authored or coauthored more than 290 research papers, including more than 150 papers in peer-reviewed journals and 140 papers in conference proceedings. His research interests include microwave photonics, which include optical generation and processing of microwave signals, ultrawideband over fiber, photonic microwave measurement, and integrated microwave photonics.

Dr. Pan is a Senior Member of the IEEE Microwave Theory and Techniques Society, IEEE Photonics Society, IEEE Instrumentation and Measurement Society, and a Fellow Member of the Optical Society of America. He was selected to receive an OSA Outstanding Reviewer Award in 2015. Dr. Pan is currently the Topical Editor of *Chinese Optics Letters*. He was the Chair of numerous international conferences and workshops, including the TPC Chair of IEEE ICOCN 2015, TPC Chair of the high-speed, and broadband wireless technologies subcommittee of the IEEE Radio Wireless Symposium in 2013, 2014, and 2016, TPC Chair of the optical fiber sensors and microwave photonics, Subcommittee Chair of the OptoElectronics and Communication Conference in 2015, the Chair of the microwave photonics for broadband measurement workshop of International Microwave Symposium in 2015, TPC Chair of the microwave photonics subcommittee of CLEO-PR, OECC and PGC 2017 (joint conference), and TPC Co-Chair of IEEE MWP 2017.